NeuroImage: Clinical 29 (2021) 102552

Contents lists available at ScienceDirect

NeuroImage: Clinical

journal homepage: www.elsevier.com/locate/ynicl

Large-scale mGluR5 network abnormalities linked to epilepsy duration in focal cortical dysplasia

Jonathan M. DuBois [a,*,1], Sulantha Mathotaarachchi [b], Olivier G. Rousset [c], Viviane Sziklas [a], Jorge Sepulcre [d,e], Marie-Christine Guiot [a,f], Jeffery A. Hall [a], Gassan Massarweh [a], Jean-Paul Soucy [g,h], Pedro Rosa-Neto [a,b,g], Eliane Kobayashi [a,*,1]

[a] Department of Neurology and Neurosurgery, Montreal Neurological Institute, McGill University, Montreal, Canada
[b] Translational Neuroimaging Laboratory, McGill Center for Studies in Aging, Douglas Mental Health University Institute, McGill University, Montreal, Canada
[c] Division of Nuclear Medicine and Molecular Imaging, Johns Hopkins University, Baltimore, United States
[d] Gordon Center for Medical Imaging, Department of Radiology, Massachusetts General Hospital, Harvard Medical School, Boston, MA, United States
[e] Athinoula A. Martinos Center for Biomedical Imaging, Department of Radiology, Massachusetts General Hospital, Harvard Medical School, Charlestown, MA, United States
[f] Department of Pathology, McGill University, Montreal, Canada
[g] PET Unit, McConnell Brain Imaging Center, Montreal Neurological Institute, McGill University, Montreal, Canada
[h] Bio-Imaging Group, PERFORM Centre, Concordia University, Montreal, Canada

ARTICLE INFO

Keywords:
mGluR5
FCD
Epilepsy
PET
Network

ABSTRACT

To determine the extent of metabotropic glutamate receptor type 5 (mGluR5) network abnormalities associated with focal cortical dysplasia (FCD), we performed graph theoretical analysis of [^{11}C]ABP688 PET binding potentials (BP_{ND}), which allows for quantification of mGluR5 availability. Undirected graphs were constructed for the entire cortex in 17 FCD patients and 33 healthy controls using inter-regional similarity of [^{11}C]ABP688 BP_{ND}. We assessed group differences in network integration between healthy controls and the ipsilateral and contralateral hemispheres of FCD patients. Compared to healthy controls, FCD patients showed reduced network efficiency and reduced small-world connectivity. The mGluR5 network of FCD patients was also less resilient to targeted removal of high centrality nodes, suggesting a less integrated network organization. In highly efficient hub nodes of FCD patients, we observed a significant negative correlation between local efficiency and duration of epilepsy only in the contralateral hemisphere, suggesting that some nodes may be more vulnerable to persistent epileptic activity. Our study provides the first in vivo evidence for a widespread reduction in cortical mGluR5 network integration in FCD patients. In addition, we find that ongoing epileptic activity may alter chemoarchitectural brain organization resulting in reduced efficiency in distant regions that are essential for network integration.

1. Introduction

Focal cortical dysplasia (FCD) is a malformation of cortical development clinically associated with drug resistant seizures. Although focal structural abnormalities are a defining characteristic of FCD, there is growing evidence that the pathophysiology of FCD may involve widespread network alterations that contribute to rapid seizure spread and incur greater functional and structural alterations due to chronic seizures (Kramer and Cash, 2012; Caciagli et al., 2014).

mGluR5 is a post-synaptic G-protein coupled receptor that may play a role in the underlying mechanism of epileptogenesis by contributing to the intrinsic epileptogenicity attributed to FCD (Palmini et al., 1995; Merlin, 2002; Aronica et al., 2003). Using [^{11}C]ABP688 PET we previously showed that, in addition to abnormal mGluR5 availability within the radiologically identified dysplasia, 80% of FCD patients had mGluR5 reductions in peri-lesional and remote regions of the cortex, which were not associated with a structural abnormality (DuBois et al., 2016a). The significance of these findings outside the epileptogenic region remain to

* Corresponding authors at: Department of Neurology and Neurosurgery, Montreal Neurological Institute and McGill University, 3801 University Street, Montreal, Quebec, H3A 2B4, Canada.
E-mail addresses: jonathan.dubois@biogen.com (J.M. DuBois), eliane.kobayashi@mcgill.ca (E. Kobayashi).
[1] This author performed the statistical analysis.

https://doi.org/10.1016/j.nicl.2020.102552
Received 27 August 2020; Received in revised form 19 December 2020; Accepted 21 December 2020
Available online 29 December 2020

be further elucidated.

While widespread functional and structural abnormalities in patients with FCD are suggestive of a system disruption, few studies have attempted to investigate the overall network organization in these patients. Graph theoretical analysis is a framework for quantification of network topology that is sensitive to distributed abnormalities in brain diseases (Rubinov and Sporns, 2010; Sporns, 2016). In two graph theory studies of patients with focal non-lesional epilepsy, resting-state fMRI showed reduced global and local efficiency, suggesting that network integration is impaired in patients with focal epilepsy (Hermann et al., 2009; Caciagli et al., 2014).

To characterize the mGluR5 network in patients with FCD, we performed graph theoretical analysis based on the inter-regional similarity of [^{11}C]ABP688 PET binding potentials (BP_{ND}). Graph metrics of network integration, including global efficiency, resilience, and local efficiency were used to compare ipsilateral and contralateral hemispheres of FCD patients to healthy controls. Based on previous studies in non-lesional focal epilepsy, we hypothesized that patients with FCD would show reduced global efficiency of mGluR5 networks.

2. Methods

2.1. Subjects

Seventeen patients with focal epilepsy previously investigated at the Montreal Neurological Hospital with an [^{11}C]ABP688 PET study were retrospectively selected for the study based on the following criteria. Patients were included if diagnosed with FCD from either MRI or neuropathology following surgery [positive MRI and neuropathological diagnosis of FCD (N = 5), positive MRI without surgery (N = 7), and negative MRI and neuropathological diagnosis of FCD (N = 5)]. FCD patients were excluded for present or past usage of illicit drugs, pregnancy/breastfeeding, or MRI contraindications. For detailed information regarding lesions location, surgical outcomes, and clinical variables, refer to Table 1.

As described previously, 33 healthy subjects were included (range = 20-77y/o; males, n = 18, 47.4 ± 17.7y/o; females, n = 15, 46.2 ± 18.9y/o) (DuBois et al., 2016a). Healthy controls were excluded from then study for any of the following: personal or first-degree relative history of axis I psychiatric disorders, chronic use of CNS active medications or illicit drugs, pregnancy/breastfeeding, present or past cigarette usage, history of neurological or medical disorders and MRI contraindications. The study was approved by the Montreal Neurological Institute Research Ethics Board. All subjects provided written informed consent prior to participation in the study.

2.2. PET acquisition and reconstruction

3-(6-methyl-pyridin-2-ylethynyl)-cyclohex-2-enone-O-^{11}C-methyl-oxime ([^{11}C]ABP688) was synthetized as previously described (Elmenhorst et al., 2010). Images were acquired in the Siemens ECAT EXACT HR + scanner for 7 patients and 7 controls [approximate resolution, 6 mm full width at half maximum (FWHM)]. The remaining subjects (10 patients and 26 controls) were scanned in the Siemens High Resolution Research Tomograph (HRRT, approximate resolution of 3 mm FWHM). A 7-minute transmission scan was performed for attenuation correction, followed by a 1-hour dynamic emission scan, which began concurrently with the slow bolus injection of [^{11}C]ABP688 (injected dose/activity = 356.7 ± 25.2 MBq; specific activity = 13.6 ± 6.3 GBq/μmol, unavailable for 10 of the controls). Data was acquired in 3D list mode and reconstructed by filtered back-projection. The reconstructed time-series was 128 × 128 × 63 voxels (2.45 mm pixels) for the HR + and 256 × 256 × 207 voxels (1.21875 mm pixels) for the HRRT. To combine data from the 2 PET scanners, HRRT images were blurred with an anisotropic Gaussian kernel of 5.7 × 5.7 × 6.7 mm FWHM.

Table 1
Clinical Information. Pat: Patient ID; F: female; M: male; L: left; R: right; Pos: positive; Neg: negative; sz: seizure; N/A: not applicable; AED: antiepileptic drug; LEV: levetiracetam, LMT: lamotrigine; CBZ: carbamazepine; CLB: clobazam; DPH: diphenylhydantoin; VA: valproic acid; TPM: topiramate; OXC: oxcarbazepine; PB: phenobarbital.

Pat	Age	Sex	FCD lobe	Radiology (MRI)	Last sz prior to scan (days)	Age at sz onset	Duration of epilepsy at the time of PET scan (years)	Surgery follow-up (years), Engel class	Pathology	AEDs
1	39	F	L frontal	Pos	180	3	36	no	N/A	LEV, LMT, CLB, CBZ
2	56	M	R parietal	Pos	1	8	48	6y, Engel I	FCD IIb	CBZ, LEV, CLB
3	25	M	R temporal	Pos	4	8	17	6y9m, Engel I	FCD IIb	CBZ
4	20	F	L temporal	Pos	1	14	6	no	N/A	CLB
5	19	F	R temporal	Pos	11	15	4	6y11m, Engel II	FCD IIa	VA, LEV, PB
6	31	F	L cingulate	Pos	1	16	15	no	N/A	LMT, DPH, CLB
7	39	F	L frontal	Pos	30	34	5	no	N/A	none
8	29	M	R frontal	Pos	1	0.4	29	4y3m, Engel I	FCD IIb	VA, OXC, CLB
9	41	F	L temporal	Pos	6	12	29	no	N/A	LMT, PB, CLB
10	38	M	R frontal	Pos	1	17	21	5y1m, Engel I	FCD IIb	CBZ, CLB
11	23	F	L cingulate	Pos	1	10	13	no	N/A	DPH, TPM
12	29	F	L parietal	Neg	120	21	8	4y, Engel II	FCD IIa	CBZ, LMT
13	35	M	R frontal	Neg	1	16	19	4y6m, Engel I	FCD IIa	LEV, TPM
14	18	F	R parietal	Neg	25	12	6	3y9m, Engel I	FCD IIb	none
15	22	F	R cingulate	Neg	14	17	5	0y1m, N/A	FCD IIa	LCM
16	25	F	R frontal	Pos	4	12	13	no	N/A	CBZ, CLB, LCM
17	41	M	R cingulate	Neg	0.5	6	35	6y11m, Engel II	FCD IIb	OXC, LEV, PB

2.3. MRI acquisition and processing

As previously described in DuBois et al. (2016a), a 3D T1-weighted MPRAGE sequence (1 mm^3 voxel size, 256 × 256 × 256 matrix; TE = 2.98; TR = 2300; TI = 900 ms; flip angle = 9°) was acquired for each subject using a Siemens Trio 3 T scanner. MRI data were analyzed with FreeSurfer (www.surfer.nmr.mgh.harvard.edu, version 6.0) (Dale et al., 1999; Fischl et al., 1999). The process included reconstruction of the pial surface and gray matter/white matter boundary (i.e. the white matter surface) (Dale et al., 1999; Fischl et al., 1999). The MRI and the time-averaged raw PET images were aligned by fitting the white matter surface to the maximum of the radioactivity gradient (Greve and Fischl, 2009). For surface-based partial volume correction and network analysis, PET data were sampled from the volume halfway between the white matter and pial surfaces using nearest-neighbor interpolation (Greve et al., 2014).

2.4. Partial volume correction and binding potential analysis

Correction for partial volume error was performed using a data-driven, region-based per-voxel partial volume correction method (DuBois et al., 2016a, 2016b). Briefly, time-averaged raw PET data were sampled to the surface and parceled into homogenous binding regions. Parcellated regions were then partial volume corrected using the geometric transfer matrix method and region-based per-voxel correction for the whole brain (Rousset et al., 1998). [^{11}C]ABP688 non-displaceable binding potentials (BP_{ND}) were estimated with a simplified reference tissue model, using the cerebellar grey matter as the reference region (DuBois et al., 2016b). Voxel-wise parametric mapping was performed using basis function implementation (Gunn et al., 1997).

2.5. Network nodes and edges

To define network nodes, we utilized an existing probabilistic atlas, which parcellated the cortex into 180 regions per hemisphere based on functional activation patterns and structural anatomy (Glasser et al., 2016). Five regions were excluded from the analysis due to increased partial volume effects around the medial wall region. Therefore, 175 regions were included in the final analysis, each representing a network node. Following binding potential analysis, BP_{ND} values were sampled from each subject's volume to the FreeSurfer surface template and extracted from each cortical region in the parcellation scheme. The probability density function was then computed for each regional BP_{ND} distribution, at the individual subject level, using kernel density estimation with automatically chosen bandwidths (function: kde, http://www.mathworks.com/matlabcentral/fileexchange/14034-kernel-density-estimator) (Wang et al., 2016). Subsequently, we compared the probability density function of each node pair by calculating Jensen-Shannon divergence (Endres and Schindelin, 2003; Kong et al., 2014). Divergence was converted to a measure of similarity (JSS), with values between 0 and 1, by taking its natural exponential (Kong et al., 2014). Hemispheric matrices were generated by dividing the whole-brain matrix into 4 quadrants and extracting left-to-left and right-to-right hemisphere node pairs (Fig. 1). Prior to network analysis, a density threshold was applied to equate the number of edges between both subjects and hemisphere matrices. The density threshold was determined by preserving a proportion of high JSS edges relative to the number of total possible edges in the matrix. All analyses were done over a broad range of densities (5% − 40%, with an interval of 1%). The resulting matrices reflect unweighted, undirected graphs.

2.6. Network analysis

We examined network topology at global and local scales for each graph. Global metrics included: small-world index, resilience, and global efficiency. Local metrics included: local efficiency and participation coefficient (PC) (Latora and Marchiori, 2001; (Blondel et al., 2008); Rubinov and Sporns, 2010). Briefly, global efficiency was defined as the average inverse of the shortest path length between all node pairs. To calculate the small-world index, characteristic path length and clustering coefficient were normalized by randomly generated networks, which preserved the number of nodes, edges, and the degree distribution of the real network. The small world index was equivalent to the normalized clustering coefficient divided by the normalized path length.

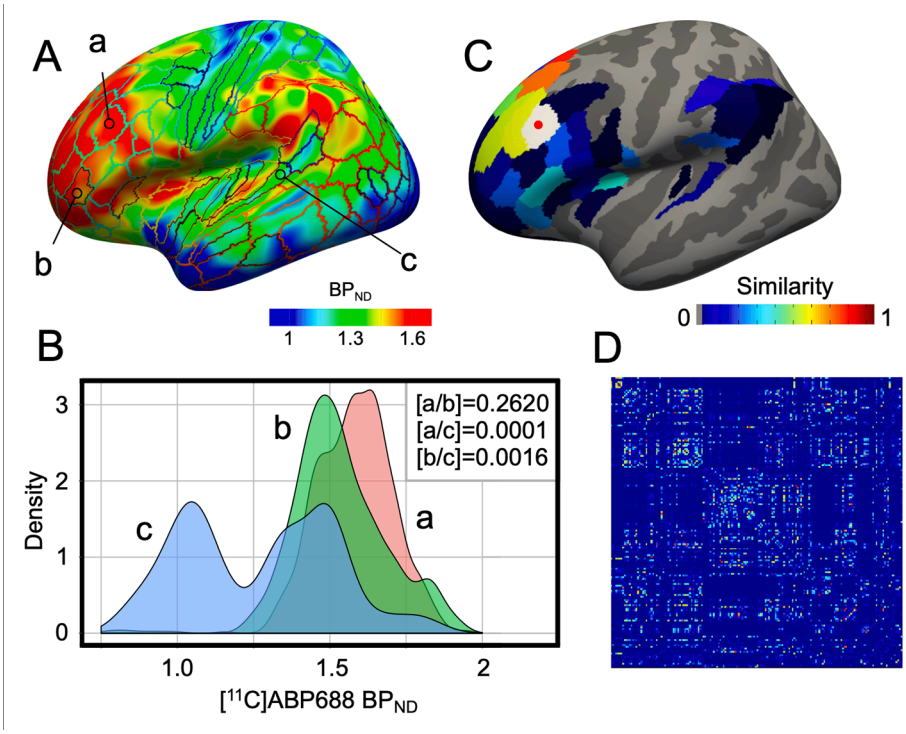

Fig. 1. Construction of network nodes and edges. Displays [^{11}C]ABP688 BP_{ND} values (unitless, ranging from 0 to 2) from a healthy control sampled to the average inflated surface with atlas regions outlined (A). Three regions of interest (ROIs) are indicated by arrows in the lateral frontal (a), orbitofrontal (b), and temporal (c) lobe, with representation of the kernel density estimate from each of the three ROIs displayed in red (a), green (b), and blue (c) (B). Atlas regions displayed on the inflated surface and colored according to their similarity to region (a) in the lateral prefrontal cortex, displayed in white with a red point (C). The square similarity matrix displaying values between 0 and 1 (D). (For interpretation of the references to colour in this figure legend, the reader is referred to the web version of this article.)

To determine the resilience of each network, we simulated attacks on the network by removing nodes, either randomly (random attack) or in descending order of their PC (targeted attack) (Albert et al., 2011). Thus, network components were incrementally removed without replacement from 0 to 100% at an increment of 1%. After each node deletion, global efficiency was recalculated (Rubinov and Sporns, 2010). All graph metrics were calculated using the Brain Connectivity Toolbox (http://www.brain-connectivity-toolbox.net) with MATLAB® (version 2015b; MathWorks) (Rubinov and Sporns, 2010).

2.7. Statistical analyses

To compare graph metrics between FCD patients and healthy controls, we calculated the area under the curve (AUC) across the density spectrum using Simpson's rule and performed non-parametric permutation tests with approximately 10,000 iterations. Pearson correlation was used to assess the relationship between graph metrics and clinical variables. False discovery rate (FDR) correction was used to control for multiple comparisons ($P < 0.05$). All analyses and figures were generated with the R statistical software package (R Development Core Team 3.0.1. 2013). In healthy controls, no significant hemispheric differences were found after FDR correction in any of the global or local network metrics. Therefore, we grouped the left and right hemispheres of healthy controls and compared graph metrics relative to the ipsilateral hemisphere (including right and left side) and contralateral hemisphere (including right and left side) of FCD patients.

3. Results

3.1. Global metrics

Global efficiency was reduced across the entire density spectrum assessed, in both the ipsilateral and contralateral hemispheres of FCD patients (Fig. 2A). Global efficiency AUC was significantly reduced in the ipsilateral ($Z = -2.78$, $P = 0.004$, *P-adjusted* $= 0.006$) and contralateral ($Z = -2.54$, $P = 0.01$, *P-adjusted* $= 0.006$) hemispheres of FCD patients (Fig. 2B). Both FCD patients and healthy controls exhibited a small-world index greater than one over the entire density spectrum, reflecting greater clustering and approximately equal path length compared to randomly generated networks (Fig. 2C). Interestingly, FCD patients showed a significantly reduced small-world index in both hemispheres (Ipsilateral: $Z = -3.09$, $P = 0.002$, *P-adjusted* $= 0.006$; Contralateral: $Z = -2.26$, $P = 0.021$, *P-adjusted* $= 0.04$ [Fig. 2D]). Overall, hemispheric graph metrics reflect a less integrated network topology in patients with FCD relative to healthy controls.

3.2. Resilience

Upon random node removal, global efficiency remained higher (greater than50% after 25% of nodes removed) than targeted removal of high PC nodes (Fig. 3), indicating that mGluR5 brain networks were resistant to random failure. Global efficiency of all groups was highly degraded by targeted removal of high PC nodes. Global efficiency was reduced by more than 50% after 25% removal of high PC nodes, and further reduced by approximately 85% after 50% removal of high PC nodes (Fig. 3).

Between-group differences of normalized global efficiency were not

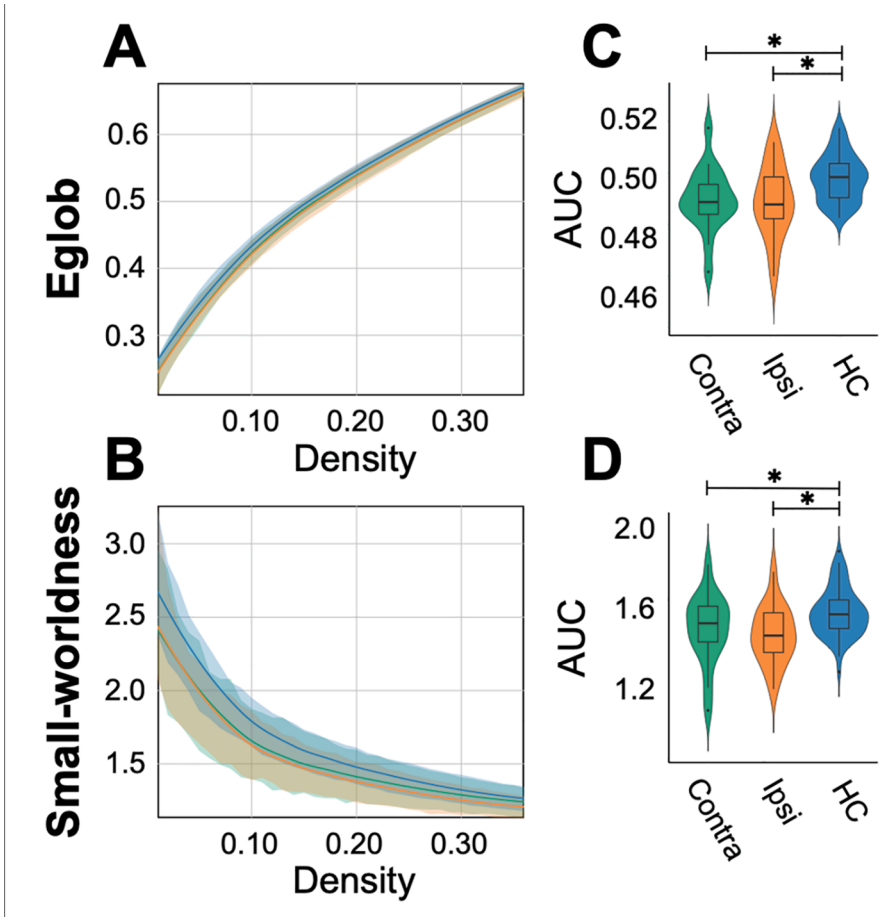

Fig. 2. Group differences in global network topology. Global efficiency (Eglob) and small-world index graphs display the fitted density curve for the contralateral (Contra) FCD hemisphere (green), ipsilateral (Ipsi) FCD hemisphere (orange), and combined hemispheres of healthy controls () (blue) (A-B). Shaded regions show one standard deviation above and below the regression line. Both graphs display a consistent difference between healthy controls and FCD patients across the density spectrum. Box-plots display the AUC across the density spectrum, with stars indicating a significant difference between healthy controls and both the ipsilateral and contralateral hemispheres of FCD patients (C-D). (For interpretation of the references to colour in this figure legend, the reader is referred to the web version of this article.)

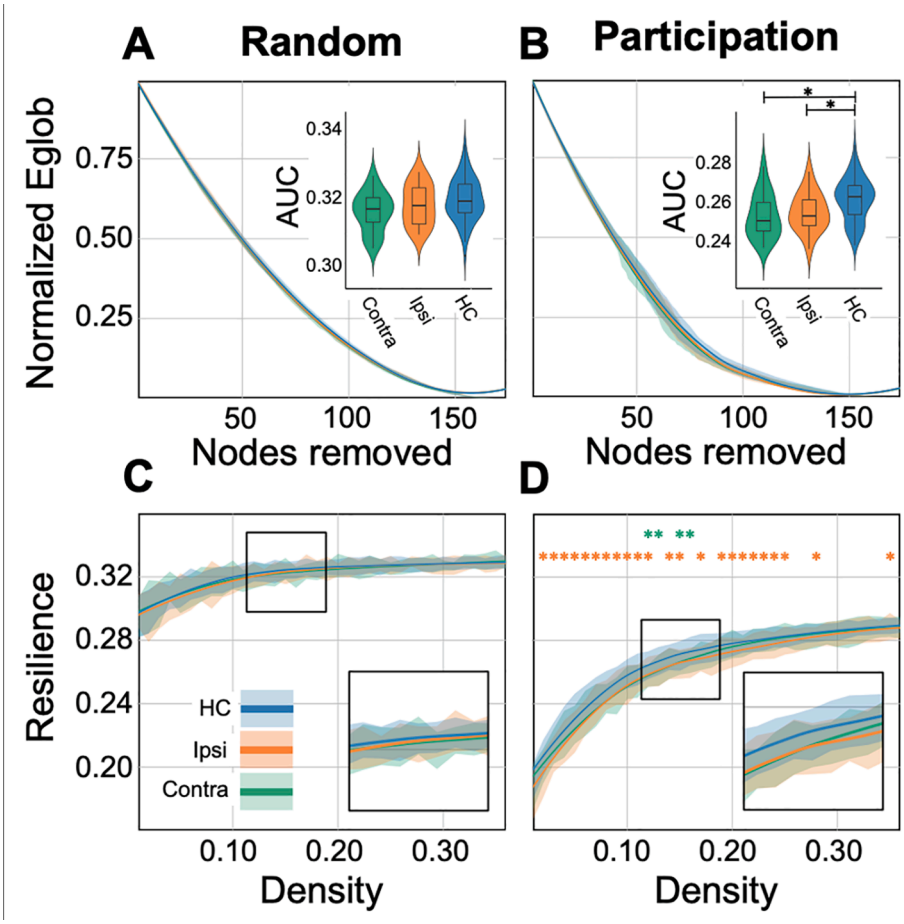

Fig. 3. Network resilience to targeted and random attack. Fitted curves display the normalized global efficiency (Eglob) on the y-axis, measured after each incremental removal of a random node (A) and high PC node (B) at a density threshold of 15%. The x-axis displays the fraction of nodes removed. Shaded regions show one standard deviation above and below the fitted curve. Box-plots indicate the AUC across the density spectrum, with the star indicating a significant difference between healthy controls (HC) (blue) and the contralateral (Contra) hemisphere (green) or ipsilateral (Ipsi) hemisphere (orange) of FCD patients. Resilience curves measure the AUC at each density threshold for the incremental removal of random (C) and PC nodes (D). Group differences were calculated at each density threshold and corrected for multiple comparisons. Significant differences are indicated by an orange (healthy controls vs. ipsilateral FCD) or green (healthy controls vs. contralateral FCD) stars. The zoomed region is centered on density thresholds between 12% and 18%, as indicated by the black box. (For interpretation of the references to colour in this figure legend, the reader is referred to the web version of this article.)

significant after random node removal at all graph densities (Fig. 3A; 2C). However, targeted removal of high PC nodes showed a significant difference in normalized global efficiency for ipsilateral (Z = -2.75, P = 0.005, *P-adjusted* = 0.006) and contralateral (Z = −3.0, P = 0.002, *P-adjusted* = 0.004) hemispheres of FCD patients compared to healthy controls at a graph density of 15% (Fig. 3D). Compared to healthy controls, ipsilateral nodes were less resistant to targeted attack across the majority of graph densities, while contralateral nodes were less resistant to targeted attack at graph densities of 11%, 12%, 14%, and 15%. Overall, graph resilience supports the above finding that the mGluR5 network is more regularized throughout the brain of patients with FCD as compared to healthy subjects.

3.3. Nodal topology

Given the previous finding of reduced global efficiency in FCD patients, we further investigated differences in nodal efficiency. In healthy controls, high efficiency nodes were observed in the precuneus, cingulate, anterior temporal, lateral parietal, and prefrontal cortices. Local efficiency was lower in FCD patients compared to healthy controls contralateral to the lesion in the anterior cingulate and prefrontal nodes, although none of these differences were significant after FDR correction.

3.4. Correlation of network metrics and demographic variables

Here, we explored the relationship between global and local network metrics with duration of epilepsy and age a seizure onset (Table 1). Seizure latency prior to PET scan and surgical outcome were not included in the analysis due to a lack of statistical power. At the local level, analyses were limited to hub nodes, defined as the top 15% of local efficiency nodes in the healthy control group, which has been used in numerous previous studies (Stanley et al., 2013). Local efficiency AUC averaged across hub nodes showed a moderately significant correlation with duration of epilepsy in the contralateral hemisphere (r(15) = −0.496, p < 0.05; [Fig. 4]), indicating that hub node efficiency may be reduced in the contralateral hemisphere in patients with a longer duration of epilepsy. A non-significant negative correlation was also observed in the contralateral hemisphere (r(15) = −0.399, p = 0.113; [Fig. 4]). No specific hub node showed a significant correlation, after multiple comparison correction, between local efficiency AUC and duration of epilepsy, indicating that the relationship was not driven by a specific node or group of nodes. In addition, none of the global metrics, including global efficiency of small word index showed a significant relationship with duration of epilepsy. For age at seizure onset, no significant correlation was found with either local or global network metrics.

4. Discussion

In the present study, we compared the network topology of mGluR5 availability between patients with FCD and healthy controls by performing graph theoretical analysis of [^{11}C]ABP688 BP_{ND} inter-regional similarity. mGluR5 brain networks in both groups showed a small-world organization, reflecting increased clustering and approximately equal path length relative to randomly organized networks (Fig. 2A and 1B). In the healthy brain, small-world networks reflect the large proportion of local intra-cortical connection relative to the small number of connections that are made between distant brain regions (Watts and Strogatz, 1998; Sporns and Zwi, 2004). While mGluR5 networks do not directly correspond to anatomical connections, through mGluR5's role

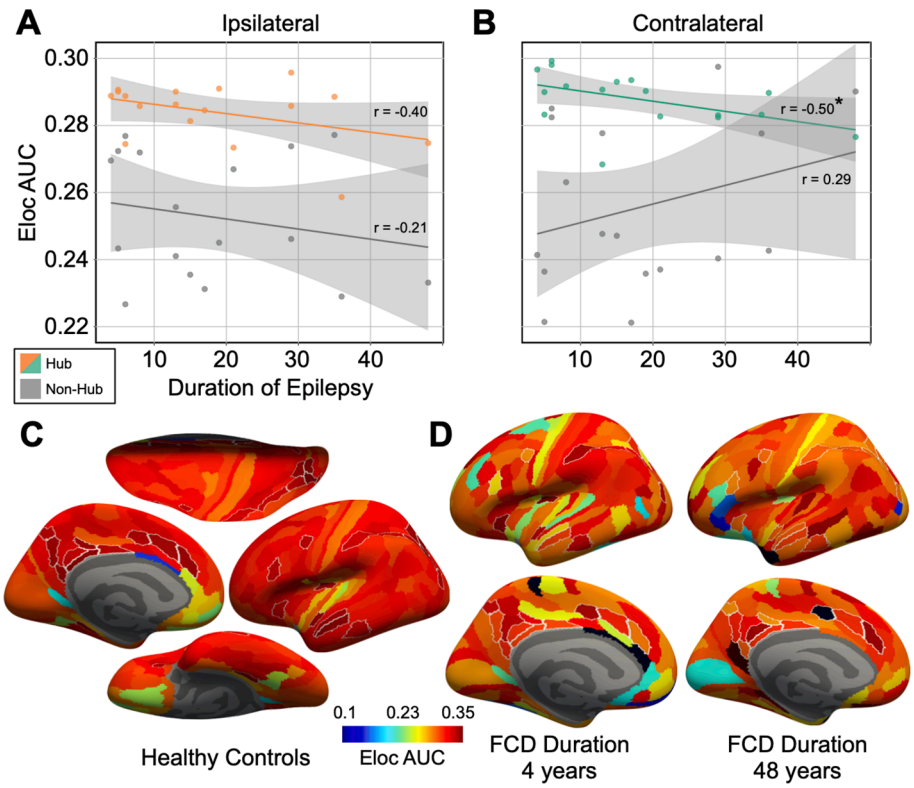

Fig. 4. Local Efficiency Correlated with Duration of Epilepsy. Scatter plot displaying the relationship between local efficiency (Eloc) in mGluR5 availability and duration of epilepsy for ipsilateral regions (A) and contralateral regions (B). Points on the graph represent the average AUC of the hub nodes (orange = ipsilateral; green = contralateral) and low efficiency nodes (gray). Hub nodes and low efficiency nodes were classified from the control group as the upper and lower 15% of local efficiency nodes. Separate lines display the linear regression for the high and low local efficiency nodes, with gray shaded regions corresponding to the 95% confidence level interval for each line. The correlation coefficient for each group is shown along the regression line, with a (*) indicating significance. The Nodal local efficiency AUC averaged across both hemispheres of the healthy control group is displayed on the inflated cortical surface (C). Brain images represent the superior (top), lateral (right), inferior (bottom), and medial (left) inflated cortical surfaces. Hub nodes are outlined in white. In two FCD patients representing the shortest (4 years) and longest (48 years) durations of epilepsy in our cohort, the nodal local efficiency AUC is displayed on the lateral (top) and medial (bottom) surfaces (D). (For interpretation of the references to colour in this figure legend, the reader is referred to the web version of this article.)

in cortical development, cell survival, and morphogenesis, the topology of mGluR5 similarity networks may resemble aspects of functional connectivity networks, as measured by resting-state fMRI (Thomas Yeo et al., 2011). mGluR5 mediates post-synaptic glutamatergic excitability, enabling long-term potentiation and long-term depression, which may reflect a small-world topology as a result of locally similar excitatory thresholds (Anwyl, 1999; Catania et al., 2007).

Within the spectrum of small-world networks, patients with FCD showed a more regularized mGluR5 topology than healthy controls, as evidenced by reduced network efficiency and reduced small-worldness in both the ipsilateral and contralateral hemispheres. In line with our findings, patients with non-lesional neocortical epilepsy have shown decreased global network efficiency using resting-state functional connectivity networks (Vlooswijk et al., 2011). Using [^{18}F] fluorodeoxyglucose (FDG) PET to assess metabolic networks, Shim et al. (2020) showed reduced network connectivity in patients with temporal lobe epilepsy with hippocampal sclerosis when compared to healthy controls. Patients with temporal lobe epilepsy additionally showed increased path length and clustering cortical thickness correlation network analysis, suggesting reduced network efficiency (Bernhardt et al., 2011). Thus, reduced network integration may be shared across several types of focal epilepsy and observable by various neuroimaging modalities.

To further understand the nature of network alterations in FCD, we assessed network resilience to attacks targeting hub nodes. While random graphs maintain high levels of global efficiency after node deletion (regardless of the centrality of the node), small-world networks are more vulnerable to deletion of high centrality nodes due to the heterogeneous distribution of connections (Achard et al., 2006; Albert et al., 2011). However, rather than a general vulnerability to deletion of high centrality nodes, patients with FCD showed a specific vulnerability to deletion of high PC nodes (Fig. 3). In contrast, global modularity, which is inversely proportional to the number of connections between modules, and therefore PC, did not significantly differ from healthy controls. These findings suggest that FCD is associated with a selective reduction in inter-modular connections, a key component of efficient networks. In patients with acquired brain injuries, a previous study using resting-state functional connectivity showed widespread differences in network modularity and integration, which were mediated by high PC nodes, or between-network connectors, rather than within-network connectors (Gratton et al., 2012). This finding is supported by previous studies using simulated network graphs to assess the effects of local lesions on global network integration (Honey and Sporns, 2008; Alstott et al., 2009). While this work underscores the importance of connector nodes to maintaining network efficiency, as FCD is a developmental disorder rather than an acquired injury, network reorganization as a result of disease duration or seizure frequency may contribute to the reduction in network integration observed in FCD.

While we did not observe group-wise differences in nodal topology, FCD patients showed an association between disease duration and local efficiency in high efficiency hub nodes contralateral to the dysplastic lesion. This suggests that ongoing seizure activity may reduce efficiency in distant regions that are essential for network integration. While significant, the correlation between local efficiency and disease duration was only moderate and was also present, to a lesser degree, in the ipsilateral hub nodes. It is likely that these analyses were limited by the small sample size and narrow range of epilepsy duration in the FCD patients included in our study. However, if confirmed by further research, these findings may support a framework in which focal lesions contribute to widespread abnormalities in chemoarchitectural brain organization via seizure propagation. While a previous study in patients with FCD did not show a relationship between disease duration and structural or functional MRI abnormalities (Hong et al., 2017), in temporal lobe epilepsy, there is growing evidence of progressive structural and functional changes beyond the epileptogenic zone. In a large sample of patients with temporal lobe epilepsy, hippocampal atrophy was evident in ipsilateral and contralateral regions of the hippocampus, amygdala and entorhinal cortex, which was more severe in patients with a seizure frequency greater than 5 per month (Bernhardt et al., 2013). In previous graph theoretical studies using electrocorticography and structural morphometry, decreased local clustering and increased path

length have been associated with a longer duration of temporal lobe epilepsy (van Dellen et al., 2009; Bernhardt et al., 2011).

Taken together, our findings of decreased resilience and decreased global efficiency underscore the presence of a less integrated network in patients with FCD. In the context of mGluR5 availability, network integration could signify a wide range of possible mechanisms, including receptor internalization, the functional state of receptor (high/low affinity), the total amount of protein in the tissue, conformational changes, anomalous receptor isoforms, or excessive concentrations of endogenous ligands (Zimmer et al., 2015; Vidal et al., 2016). We have previously suggested that reduced mGluR5 availability in the lesion, assessed in vivo with [^{11}C]ABP688 PET, may be related to increased glutamate concentrations, which when bound to the orthosteric site can cause a conformational change in mGluR5, making the transmembrane allosteric site unavailable for [^{11}C]ABP688 binding (DeLorenzo et al., 2015; Zimmer et al., 2015). While microdialysis studies have shown that extracellular glutamate concentrations in the seizure focus are elevated interictally (Çavuş et al., 2016), glutamate concentrations beyond the epilepsy focus as measured by microdialysis remain unknown. It is possible that glutamate concentration may be increased in the seizure focus due to recurrent and persistent epileptogenic activity, whereas mGluR5 may be internalized in brain regions associated with network integration as a compensatory mechanism. Both internalization and increased glutamate concentration may lead to reduced mGluR5 availability as measured by [^{11}C]ABP688 PET.

The main limitation of this work was the small number of patients evaluated and the variable anatomical locations of the FCD lesions. A larger patient population would provide greater control for potential confounds relevant to mGluR5 PET imaging, such as cigarette smoking, psychiatric disorders, antiepileptic drug load, and sleep deprivation (Akkus et al., 2013; Hefti et al., 2013). In addition, understanding the relationship between surgical outcomes and widespread network abnormalities may allow for better surgical planning. Of the three FCD patients with an Engel class higher than one, none were found to be outliers in any of the global or local network metrics, although we were unable to examine seizure outcome systematically due to a lack of statistical power. Similarly, we were not able to investigate the association between seizure latency prior to the PET scan and local and global efficiency in the FCD patients, as 65% of patients had a seizure within 6 days of the PET scan. As described above, mGluR5 availability, and by extension global and local network efficiency, may be affected by extracellular glutamate, which is increased by seizures. While the association between hub node local efficiency and duration of epilepsy shown here would contradict short-term changes in mGluR5 network metrics due to a recent seizure, differences in long-term seizure frequency may affect network efficiency and resilience. Unfortunately, accurate estimates of seizure frequency are difficult to obtain prior to hospital admission. Future research with a larger FCD population should attempt to address seizure frequency, seizure latency prior to scanning, surgical outcomes, and other clinical and demographic variables relevant to FCD.

In conclusion, we provide the first evidence for widespread mGluR5 network abnormalities in patients with FCD. Our findings of bilaterally reduced network efficiency and resilience supports the notion that mGluR5 networks are less integrated in patients with FCD relative to healthy controls. In addition, the association between duration of epilepsy and reduced efficiency in contralateral hub nodes suggests a progressive decline in mGluR5 network integration. Our findings support the concept that FCD may be better characterized as a system-wide disorder, rather than a focal abnormality, from a glutamatergic neuroreceptor perspective. Further research is needed to determine if other forms of focal epilepsy also exhibit network-wide glutamatergic alterations. Furthermore, the graph theoretic approach employed here allows for neuroreceptor systems that can be imaged with PET to be compared to other measures of functional and structural connectivity. This multimodal approach may indeed provide a more comprehensive description of network alterations that sub-serve clinical presentation of brain malformations (including seizures) and lead to novel diagnostic and therapeutic applications.

CRediT authorship contribution statement

Jonathan M. DuBois: Conceptualization, Methodology, Formal analysis, Investigation, Writing - original draft, Writing - review & editing, Visualization. **Sulantha Mathotaarachchi:** Methodology, Formal analysis, Writing - original draft, Visualization. **Olivier G. Rousset:** Methodology, Software, Validation, Writing - original draft, Writing - review & editing, Visualization. **Viviane Sziklas:** Methodology, Software, Validation, Writing - original draft, Writing - review& editing, Visualization. **Jorge Sepulcre:** Writing - original draft, Supervision. **Marie-Christine Guiot:** Methodology, Investigation, Writing - original draft. **Jeffery A. Hall:** Methodology, Investigation, Writing - original draft. **Gassan Massarweh:** Methodology, Writing - original draft. **Jean-Paul Soucy:** . **Pedro Rosa-Neto:** Conceptualization, Writing - original draft, Supervision, Funding acquisition. **Eliane Kobayashi:** Conceptualization, Writing - original draft, Writing - review & editing, Supervision, Funding acquisition.

Acknowledgements

The study was supported by the Savoy Foundation for Epilepsy (www.savoy-foundation.ca) (pilot project grant to EK and PRN and PhD studentship to JMD), and partially by the American Epilepsy Society (www.aesnet.org) (Early Career Physician Scientist Award to EK), Canadian Institutes of Health Research (CIHR) (www.cihr-irsc.gc.ca) [MOP-115131 to PRN and MOP-93614 to EK], and the Fonds de la recherche en santé du Québec (www.frqs.gouv.qc.ca) (PRN, chercheur boursier).

References

Achard, S., Salvador, R., Whitcher, B., Suckling, J., Bullmore, E., 2006. A resilient, low-frequency, small-world human brain functional network with highly connected association cortical hubs. J Neurosci. 26, 63–72.

Akkus, F., Ametamey, S.M., Treyer, V., Burger, C., Johayem, A., Umbricht, D., Gomez Mancilla, B., Sovago, J., Buck, A., Hasler, G., 2013. Marked global reduction in mGluR5 receptor binding in smokers and ex-smokers determined by [11C]ABP688 positron emission tomography. Proc. Natl. Acad. Sci. 110 (2), 737–742. https://doi.org/10.1073/pnas.1210984110.

Albert, R., Jeong, H., Barabási, A.L., 2011. Error and attack tolerance of complex networks. Struct Dyn Networks. 503–506, 9781400841.

Alstott J, Breakspear M, Hagmann P, Cammoun L, Sporns O. 2009. Modeling the impact of lesions in the human brain. PLoS Comput. Biol. 5:e1000408.

Anwyl, R., 1999. Metabotropic glutamate receptors: electrophysiological properties and role in plasticity. Brain Res. Rev. 29 (1), 83–120. https://doi.org/10.1016/S0165-0173(98)00050-2.

Aronica, E., Gorter, J.A., Jansen, G.H., Van Veelen, C.W.M., Van Rijen, P.C., Ramkema, M., Troost, D., 2003. Expression and cell distribution of group I and group II metabotropic glutamate receptor subtypes in taylor-type focal cortical dysplasia. Epilepsia 44, 785–795.

Bernhardt, B.C., Chen, Z., He, Y., Evans, A.C., Bernasconi, N., 2011. Graph-theoretical analysis reveals disrupted small-world organization of cortical thickness correlation networks in temporal lobe epilepsy. Cereb. Cortex. 21, 2147–2157.

Bernhardt, B.C., Hong, S., Bernasconi, A., Bernasconi, N., 2013. Imaging structural and functional brain networks in temporal lobe epilepsy. Front. Hum Neurosci.

Blondel, V.D., Guillaume, J.L., Lambiotte, R., Lefebvre, E., 2008. Fast unfolding of communities in large networks. J. Stat. Mech. Theory Exp. 2008.

Caciagli, L., Bernhardt, B.C., Hong, S.-J., Bernasconi, A., Bernasconi, N., 2014. Functional network alterations and their structural substrate in drug-resistant epilepsy. Front Neurosci. 8, 411.

Catania, M.V., D'Antoni, S., Bonaccorso, C.M., Aronica, E., Bear, M.F., Nicoletti, F., 2007. Group I metabotropic glutamate receptors: a role in neurodevelopmental disorders? Mol Neurobiol. 35, 298–307.

Çavuş, I., Romanyshyn, J.C., Kennard, J.T., Farooque, P., Williamson, A., Eid, T., Spencer, S.S., Duckrow, R., Dziura, J., Spencer, D.D., 2016. Elevated basal glutamate and unchanged glutamine and GABA in refractory epilepsy: Microdialysis study of 79 patients at the yale epilepsy surgery program: glutamate, Glutamine, and GABA in Refractory Epilepsy. Ann Neurol. 80 (1), 35–45. https://doi.org/10.1002/ana.24673.

Dale, A.M., Fischl, B., Sereno, M.I., 1999. Cortical surface-based analysis. NeuroImage 9 (2), 179–194. https://doi.org/10.1006/nimg.1998.0395.

DeLorenzo, C., DellaGioia, N., Bloch, M., Sanacora, G., Nabulsi, N., Abdallah, C., Yang, J., Wen, R., Mann, J.J., Krystal, J.H., Parsey, R.V., Carson, R.E., Esterlis, I., 2015. In vivo ketamine-induced changes in [11 C]ABP688 binding to metabotropic glutamate receptor subtype 5. Biol. Psychiatry 77 (3), 266–275. https://doi.org/10.1016/j.biopsych.2014.06.024.

DuBois, J.M., Rousset, O.G., Guiot, M.-C., Hall, J.A., Reader, A.J., Soucy, J.-P., Rosa-Neto, P., Kobayashi, E., 2016a. Metabotropic glutamate receptor type 5 (mGluR5) cortical abnormalities in focal cortical dysplasia identified in vivo with [11 C]ABP688 positron-emission tomography (PET) imaging. Cereb. Cortex 26 (11), 4170–4179. https://doi.org/10.1093/cercor/bhw249.

DuBois, J.M., Rousset, O.G., Rowley, J., Porras-Betancourt, M., Reader, A.J., Labbe, A., Massarweh, G., Soucy, J.-P., Rosa-Neto, P., Kobayashi, E., 2016b. Characterization of age/sex and the regional distribution of mGluR5 availability in the healthy human brain measured by high-resolution [11C]ABP688 PET. Eur. J. Nucl. Med. Mol. Imaging 43 (1), 152–162. https://doi.org/10.1007/s00259-015-3167-6.

Elmenhorst, D., Minuzzi, L., Aliaga, A., Rowley, J., Massarweh, G., Diksic, M., Bauer, A., Rosa-Neto, P., 2010. In vivo and in vitro validation of reference tissue models for the mGluR 5 Ligand [11 C]ABP688. J. Cereb. Blood Flow Metab. 30 (8), 1538–1549. https://doi.org/10.1038/jcbfm.2010.65.

Endres, D.M., Schindelin, J.E., 2003. A new metric for probability distributions. IEEE Trans. Inform. Theory 49 (7), 1858–1860. https://doi.org/10.1109/TIT.2003.813506.

Fischl, B., Sereno, M.I., Dale, A.M., 1999. Cortical surface-based analysis. NeuroImage 9 (2), 195–207. https://doi.org/10.1006/nimg.1998.0396.

Glasser, M.F., Coalson, T.S., Robinson, E.C., Hacker, C.D., Harwell, J., Yacoub, E., Ugurbil, K., Andersson, J., Beckmann, C.F., Jenkinson, M., Smith, S.M., Van Essen, D. C., 2016. A multi-modal parcellation of human cerebral cortex. Nature 536 (7615), 171–178. https://doi.org/10.1038/nature18933.

Gratton, C., Nomura, E.M., Pérez, F., D'Esposito, M., 2012. Focal brain lesions to critical locations cause widespread disruption of the modular organization of the brain. J. Cognit. Neurosci. 24 (6), 1275–1285. https://doi.org/10.1162/jocn_a_00222.

Greve, D.N., Fischl, B., 2009. Accurate and robust brain image alignment using boundary-based registration. NeuroImage 48 (1), 63–72. https://doi.org/10.1016/j.neuroimage.2009.06.060.

Greve, D.N., Svarer, C., Fisher, P.M., Feng, L., Hansen, A.E., Baare, W., Rosen, B., Fischl, B., Knudsen, G.M., 2014. Cortical surface-based analysis reduces bias and variance in kinetic modeling of brain PET data. NeuroImage 92, 225–236. https://doi.org/10.1016/j.neuroimage.2013.12.021.

Gunn, R.N., Lammertsma, A.A., Hume, S.P., Cunningham, V.J., 1997. Parametric imaging of ligand-receptor binding in PET using a simplified reference region model. NeuroImage 6 (4), 279–287. https://doi.org/10.1006/nimg.1997.0303.

Hefti, K., Holst, S.C., Sovago, J., Bachmann, V., Buck, A., Ametamey, S.M., Scheidegger, M., Berthold, T., Gomez-Mancilla, B., Seifritz, E., Landolt, H.-P., 2013. Increased metabotropic glutamate receptor subtype 5 availability in human brain after one night without sleep. Biol. Psychiatry 73 (2), 161–168. https://doi.org/10.1016/j.biopsych.2012.07.030.

Hermann, B.P., Lin, J.J., Jones, J.E., Seidenberg, M., 2009. The emerging architecture of neuropsychological impairment in epilepsy. Neurol. Clin. 27 (4), 881–907. https://doi.org/10.1016/j.ncl.2009.08.001.

Honey, C.J., Sporns, O., 2008. Dynamical consequences of lesions in cortical networks. Hum. Brain Mapp. 29 (7), 802–809. https://doi.org/10.1002/hbm.20579.

Hong, S.J., Bernhardt, B.C., Gill, R.S., Bernasconi, N., Bernasconi, A., 2017. The spectrum of structural and functional network alterations in malformations of cortical development. Brain 140, 2133–2143.

Kong, X.-Z., Wang, X., Huang, L., Pu, Y.i., Yang, Z., Dang, X., Zhen, Z., Liu, J., 2014. Measuring individual morphological relationship of cortical regions. J. Neurosci. Methods 237, 103–107. https://doi.org/10.1016/j.jneumeth.2014.09.003.

Kramer, M.A., Cash, S.S., 2012. Epilepsy as a disorder of cortical network organization. Neuroscientist 18 (4), 360–372. https://doi.org/10.1177/1073858411422754.

Latora, V., Marchiori, M., 2001. Efficient behavior of small-world networks. Phys. Rev. Lett. 87 (19) https://doi.org/10.1103/PhysRevLett.87.198701.

Merlin, L.R., 2002. Differential roles for mGluR1 and mGluR5 in the persistent prolongation of epileptiform bursts. J. Neurophysiol. 87 (1), 621–625. https://doi.org/10.1152/jn.00579.2001.

Palmini, A., Gambardella, A., Andermann, F., Dubeau, F., da Costa, J.C., Olivier, A., Tampieri, D., Gloor, P., Quesney, F., Andermann, E., Paglioli, E., Paglioli-Neto, E., Andermann, L.C., Leblanc, R., Kim, H.-I., 1995. Intrinsic epileptogenicity of human dysplastic cortex as suggested by corticography and surgical results. Ann Neurol. 37 (4), 476–487. https://doi.org/10.1002/ana.410370410.

R Development Core Team 3.0.1. 2013. A Language and Environment for Statistical Computing. R Found Stat Comput. 2:https://www.R-project.org.

Rousset, O.G., Ma, Y., Evans, A.C., 1998. Correction for partial volume effects in PET: principle and validation. J. Nucl. Med. 39, 904–911.

Rubinov, M., Sporns, O., 2010. Complex network measures of brain connectivity: uses and interpretations. NeuroImage 52 (3), 1059–1069. https://doi.org/10.1016/j.neuroimage.2009.10.003.

Shim, H.-K., Lee, H.-J., Kim, S.E., Lee, B.I., Park, S., Park, K.M., 2020. Alterations in the metabolic networks of temporal lobe epilepsy patients: a graph theoretical analysis using FDG-PET. NeuroImage: Clinical 27, 102349. https://doi.org/10.1016/j.nicl.2020.102349.

Sporns, O., 2016. Micro-, Meso- and Macro-Connectomics of the Brain. Springer, pp. 107–127.

Sporns O, Zwi JD. 2004. The small world of the cerebral cortex. Neuroinformatics. 2: 145–162.

Stanley, M.L., Moussa, M.N., Paolini, B.M., Lyday, R.G., Burdette, J.H., Laurienti, P.J., 2013. Defining nodes in complex brain networks. Front. Comput. Neurosci. 7, 169.

van Dellen, E., Douw, L., Baayen, J.C., Heimans, J.J., Ponten, S.C., Vandertop, W.P., Velis, D.N., Stam, C.J., Reijneveld, J.C., 2009. Long-term effects of temporal lobe epilepsy on local neural networks: a graph theoretical analysis of corticography recordings. PLoS One 4 e8081.

Vidal, B., Sebti, J., Verdurand, M., Fieux, S., Billard, T., Streichenberger, N., Troakes, C., Newman-Tancredi, A., Zimmer, L., 2016. Agonist and antagonist bind differently to 5-HT1A receptors during Alzheimer's disease: a post-mortem study with PET radiopharmaceuticals. Neuropharmacology 109, 88–95. https://doi.org/10.1016/j.neuropharm.2016.05.009.

Vlooswijk, M.C.G., Vaessen, M.J., Jansen, J.F.A., de Krom, M.C.F.T.M., Majoie, H.J.M., Hofman, P.A.M., Aldenkamp, A.P., Backes, W.H., 2011. Loss of network efficiency associated with cognitive decline in chronic epilepsy. Neurology 77 (10), 938–944. https://doi.org/10.1212/WNL.0b013e31822cfc2f.

Wang, H., Jin, X., Zhang, Y., Wang, J., 2016. Single-subject morphological brain networks: connectivity mapping, topological characterization and test-retest reliability. Brain Behav. 6, e00448.

Watts, D.J., Strogatz, S.H., 1998. Collective dynamics of 'small-world' networks. Nature 393 (6684), 440–442. https://doi.org/10.1038/30918.

Thomas Yeo, B.T., Krienen, F.M., Sepulcre, J., Sabuncu, M.R., Lashkari, D., Hollinshead, M., Roffman, J.L., Smoller, J.W., Zöllei, L., Polimeni, J.R., Fischl, B., Liu, H., Buckner, R.L., 2011. The organization of the human cerebral cortex estimated by intrinsic functional connectivity. J. Neurophysiol. 106 (3), 1125–1165. https://doi.org/10.1152/jn.00338.2011.

Zimmer, E.R., Parent, M.J., Leuzy, A., Aliaga, A., Aliaga, A., Moquin, L., Schirrmacher, E. S., Soucy, J.-P., Skelin, I., Gratton, A., Gauthier, S., Rosa-Neto, P., 2015. Imaging in vivo glutamate fluctuations with [11 C]ABP688: a GLT-1 challenge with ceftriaxone. J. Cereb. Blood Flow Metab. 35 (7), 1169–1174. https://doi.org/10.1038/jcbfm.2015.35.